European Journal of Nuclear Medicine and Molecular Imaging (2026) 53:7514–7526
https://doi.org/10.1007/s00259-026-08083-y

ORIGINAL ARTICLE

Personalized metabolic connectome analysis reveals glucose heterogeneity in ischemic cerebrovascular disease

Bixiao Cui[1,2,3,4] · Qi Zhang[5,6] · Yi Shan[1,3,4] · Xinyu Wei[6] · Yaqi Xu[6] · Jie Ma[1,2,3] · Juanjuan Jiang[7] · Luyao Wang[6] · Matthias Brendel[8,9,10] · Axel Rominger[11] · Kuangyu Shi[11,12] · Min Wang[6] · Jiehui Jiang[6] · Jie Lu[1,3,4]

Received: 15 April 2026 / Accepted: 13 July 2026 / Published online: 22 July 2026
© The Author(s), under exclusive licence to Springer-Verlag GmbH Germany, part of Springer Nature 2026

Abstract

Purpose This study aimed to establish individualized metabolic networks for patients with ischemic cerebrovascular disease (ICVD) using cerebral glucose metabolism data and to analyze topological alterations before and after surgical intervention.

Methods We enrolled 31 surgically treated ICVD patients with unilateral cerebral infarction (21 with complete postoperative follow-up) and 17 normal controls (NC). We constructed individualized brain metabolic networks from [^{18}F]-fluoro-2-deoxy-D-glucose positron emission tomography ([^{18}F]FDG PET) scans using Kullback-Leibler divergence. In the NC group, subnetworks were defined as the left intrahemispheric, right intrahemispheric and interhemispheric networks. In the ICVD group, after hemispheric alignment based on the surgical side, subnetworks were redefined as the surgical intrahemispheric, non-surgical intrahemispheric, and interhemispheric networks. Then, graph-theoretical parameters were calculated to derive the metabolic connectivity expression score (MCES). Finally, we used Kruskal-Wallis tests, paired t-tests, and Spearman correlation analysis to assess topological differences and their relationship with National Institutes of Health Stroke Scale (NIHSS) scores.

Results The preoperative ICVD group showed significantly altered metabolic connectivity compared with controls, with higher global MCES values (0.83 vs. 0.32, $p<0.0001$). Ipsilesional subnetworks exhibited reduced connectivity, whereas contralesional subnetworks showed increased connectivity. Subnetwork analysis showed that the interhemispheric network in the ICVD group had a mean MCES of 0.91, which was significantly higher than that of the interhemispheric network in the NC group (0.17, $p<0.0001$). Postoperatively, network connectivity showed partial recovery, particularly within the interhemispheric network. MCES was significantly correlated with NIHSS scores in the global, non-surgical intrahemispheric, and interhemispheric networks ($|r|=0.58\sim0.65$, $p<0.05$), but not in the surgical intrahemispheric network.

Conclusion ICVD is associated with disrupted metabolic connectivity that exhibits early postoperative remodeling following surgical revascularization. Changes in interhemispheric network topology may provide insight into early postoperative metabolic network reorganization.

Keywords Ischemic cerebrovascular disease · Personalized metabolic network · [^{18}F]FDG PET · Graph Theory · Network Reorganization

Background

Ischemic cerebrovascular disease (ICVD), a major disease that seriously endangers human health, remains one of the leading causes of global mortality and long-term disability and is characterized by high incidence, recurrence, and morbidity rates [1, 2]. Neural remodeling refers to dynamic changes in the brain's structure and function that enable adaptation to learning, memory, environmental stimuli, and other physiological demands. It involves alterations in the number and morphology of neuronal nuclei, as well as modifications in multiple neural functions and their interconnections [3, 4]. In ICVD, endogenous plasticity-driven remodeling of cerebral metabolism and functional connectivity serves as an adaptive mechanism through which the brain compensates for focal injury and strives to restore neural function [5]. Clinically, accurate monitoring and interpretation of this remodeling process remains a key

Bixiao Cui, Qi Zhang and Yi Shan contributed equally to this work.

Extended author information available on the last page of the article

challenge and an active research focus in neuroscience, as its patterns and extent are directly correlated with patients' functional recovery and long-term prognosis.

Cerebral metabolic alterations serve as pivotal indicators for evaluating brain function in patients with ICVD and can be robustly quantified using [^{18}F]-fluoro-2-deoxy-D-glucose positron emission tomography ([^{18}F]FDG PET) [6–8]. Although the standardized uptake value ratio (SUVR) is widely used, it only reflects local metabolic activity in isolation, making it difficult to interpret the integrity of brain function and to capture metabolic synergies among distributed neural networks. This synergistic interaction represents a pivotal indicator of neural remodeling. An expanding body of evidence demonstrates that metabolic coupling among brain regions is fundamental to sustaining cerebral homeostasis and underpins the pathophysiological mechanisms of neurological disorders [9–12]. Dynamic reorganization of brain metabolic networks serves as a direct, quantifiable reflection of both the magnitude and directional of neural remodeling: following cerebral ischemia, functional compensation is achieved through adaptive neural remodeling processes, together with structural and functional reconfiguration of metabolic networks and shifts in interregional metabolic synergy. Unilateral cerebral infarction triggers intrinsic compensatory mechanisms involving metabolic and functional reorganization.

The advent of brain network analysis has enabled a systems-level exploration of neural function. Emerging evidence shows that ischemic stroke induces not only focal damage but also global perturbations in connectivity. This network reorganization is widely believed to reflect the brain's intrinsic compensatory mechanisms [13, 14], serving as a key factor in determining functional recovery and explaining interindividual variability in prognosis. This topological approach offers deeper insights into neurological pathology [15]. [^{18}F]FDG PET-based metabolic connectome analysis has proved effective in characterizing such network-level alterations in various neurological disorders [16–19]. The metabolic connectome affords a comprehensive characterization of glucose metabolic disruptions across peri-infarct territories and the contralesional hemisphere in cerebrovascular disease, with particular emphasis on assessing treatment-associated metabolic recovery through large-scale network reorganization. Building on this, our previous work proposed an individual-level metabolic connectome framework that overcomes the limitations of conventional group-based indices. This data-driven approach, combined with graph theory, allows systematic quantification of functional damage and compensatory remodeling in cerebrovascular disease.

In this study, we constructed individualized metabolic networks for patients with ICVD using [^{18}F]FDG PET data. By comparing topological properties across preoperative, postoperative, and control groups, we aimed to elucidate the patterns of metabolic remodeling associated with ICVD.

Materials and methods

Participants

This study enrolled 31 patients with ICVD and 17 normal controls (NC) from the Department of Radiology and Nuclear Medicine at Xuanwu Hospital, Capital Medical University. All patients were diagnosed with symptomatic unilateral steno-occlusive disease of the internal carotid artery (ICA) or middle cerebral artery (MCA) and underwent superficial temporal artery-middle cerebral artery (STA-MCA) bypass surgery. Among them, 21 patients completed postoperative imaging within two weeks and were included in the longitudinal subgroup analysis. Disease severity was assessed using the National Institutes of Health Stroke Scale (NIHSS) and the modified Rankin Scale (mRS). The detailed inclusion and exclusion criteria can be found in the previous literature [20].

This retrospective study was approved by the ethics committee and institutional review board of Xuanwu Hospital (Approval number: [2025]286-002) and was conducted in accordance with the principles of the Declaration of Helsinki. Written informed consent was obtained from all participants before the examinations. The experimental framework of this study is shown in Fig. 1.

PET/MR acquisition protocol

Multiple MRI sequences included a T1-weighted MRI sequence for the anatomic localization (voxel size, $1 \times 1 \times 1$ mm; echo time (TE), 3.2 ms; repetition time (TR), 8.5 ms; matrix, 256×256; 178 slices); MRA sequence for the segmentation of the internal carotid vasculature (voxel size, $0.43 \times 0.43 \times 0.7$ mm; TE, 3.7 ms; TR, 25 ms; matrix, 512×512; 272 slices); and a T2 fluid-attenuated inversion recovery (FLAIR) sequence for the definition of infarct areas (voxel size, $0.47 \times 0.47 \times 4$ mm; TE, 144 ms; TR, 11000 ms; matrix, 512×512; 32 slices). PET acquisition was simultaneously initiated with manual intravenous injection of [^{18}F]FDG (3.7 MBq/kg), and a single static PET frame was reconstructed (50–60 min, voxel size: $1.82 \times 1.82 \times 2.78$ mm; matrix, 192×192; 89 slices). Detailed collection parameters can be obtained from previous literature [20].

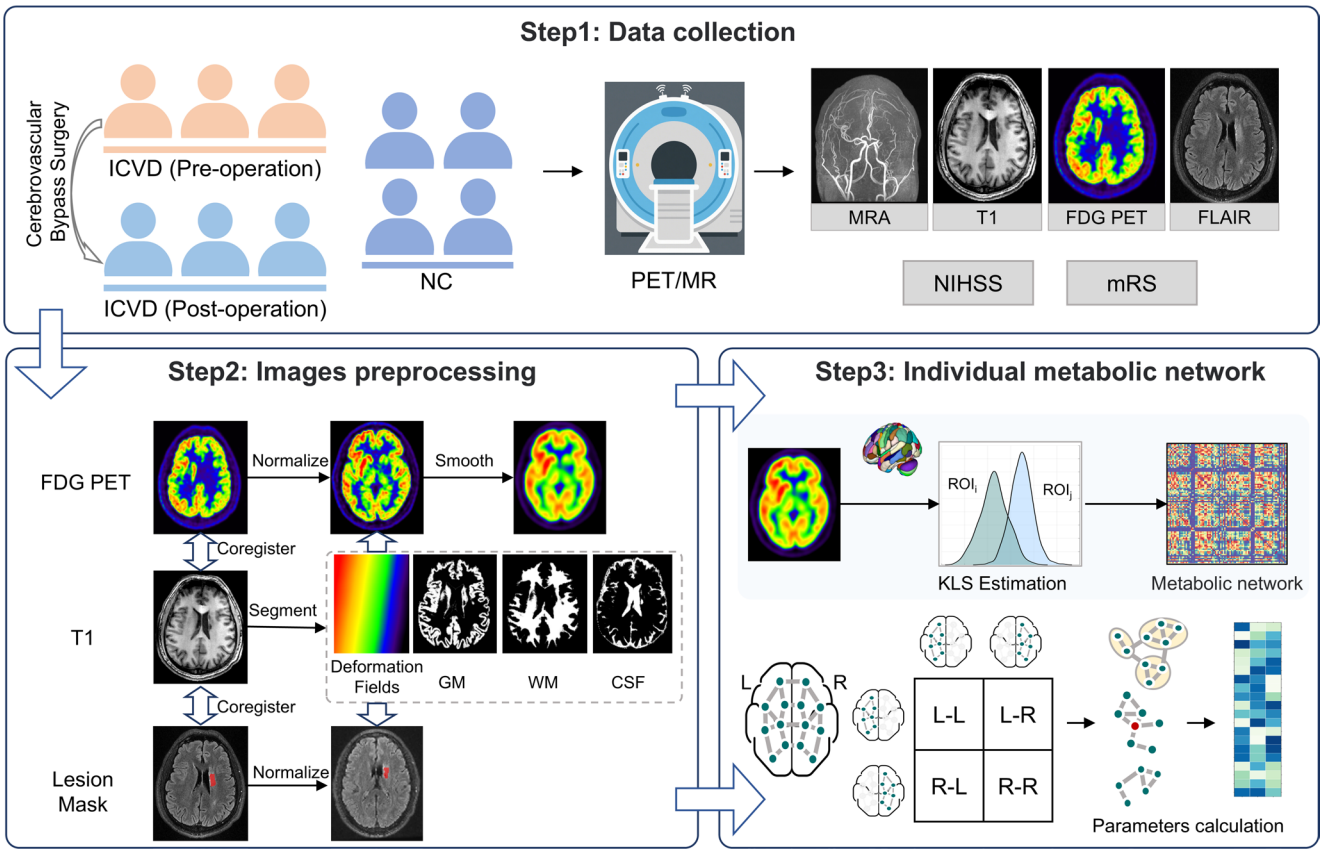


Fig. 1 Research workflow

Image preprocessing

The infarct region of each patient was generated by averaging the results from two experienced radiologists, each of whom independently reviewed the infarct areas on the original FLAIR images (double-blinded evaluation), as previously described [21].

The preprocessing procedures were performed using Statistical Parametric Mapping software (SPM12; Wellcome Centre for Human Neuroimaging, London, UK) implemented in MATLAB (R2022b; MathWorks, Natick, MA, USA). Each [^{18}F]FDG PET image and lesion mask image was coregistered to the corresponding T1-weighted MRI image. Then, the MRI images were segmented into gray matter, white matter, and cerebrospinal fluid tissue probability maps using the unified segmentation method. The registered PET image and lesion mask image were spatially normalized to Montreal Neurological Institute space using the transformation parameters. Lastly, PET images were smoothing using an 8 mm full-width at half-maximum Gaussian kernel to enhance signal-to-noise ratios. Notably, all [^{18}F]FDG PET images underwent count normalization using pons uptake and were further generated standard uptake value ratio (SUVR) images [20, 21].

Global network topological identification

Brain nodes were defined using 90 cerebral regions of interest (ROIs) from the Automated Automatic Labeling (AAL) atlas [22]. To construct individual metabolic networks, we employed the Kullback-Leibler divergence similarity estimation (KLSE) method, a technique previously established by our group [10]. Specifically, voxel intensities were extracted from preprocessed [^{18}F]FDG PET images for each ROI. Kernel density estimation was then applied to estimate the probability density function (PDF) for each region. Subsequently, KL divergence was calculated to quantify the metabolic similarity between pairwise regions, yielding an undirected adjacency matrix for each participant that represented the global metabolic network and was further used for topological parameters analysis.

Topological parameters analysis

First, topological metrics, including betweenness (B), clustering coefficient (C), degree (D), global efficiency (E_{global}), local efficiency (E_{local}), shortest path length (L_p), modularity (M), and hierarchical coefficient (H), were calculated using GRETNA (https://www.nitrc.org/projects/gretna/).

The above eight topological parameters were extracted from the metabolic connectivity networks for each subject. Second, the extracted topological parameters were organized into a feature matrix, with each row representing a subject and each column representing a topological feature. Third, a binary logistic regression model was established, with the study group (e.g., patient vs. control) defined as the dependent variable. The eight topological parameters were simultaneously entered into the logistic regression model as independent variables. No additional feature selection procedure was performed. Fourth, regression coefficients were estimated using all available subjects, and the fitted probability of belonging to the patient group was calculated for each subject based on the fitted model. Given the exploratory nature of this study and the limited sample size, cross-validation was not performed. Fifth, the fitted probability generated by the logistic regression model was defined as the MCES. Additionally, the asymmetry index (AI) was calculated from SUVR maps. To ensure accuracy, the infarct lesion and its homologous contralateral region were masked out. The mean AI was then computed for group comparison.

The subnetworks were extracted from the global network based on anatomical laterality in the NC group. Accordingly, the subnetworks were designated as follows: (1) the L-L network, representing the left-left intrahemispheric network; (2) the R-R network, representing the right intrahemispheric network; (3) the L-R network, representing interhemispheric network. As the connectivity matrices are symmetric, the L-R and R-L networks are identical; therefore, the term L-R network is used throughout this study. All the topological metrics described above were also computed in all subnetworks.

For patients with ICVD, to account for lesion distribution, the hemispheres were reclassified as the surgical hemisphere (S) and the non-surgical hemisphere (N). To facilitate group-level longitudinal analysis and ensure hemispheric consistency across patients with left- and right-sided infarctions, images from patients with left-hemisphere lesions were flipped along the midsagittal plane, such that the lesion side was consistently aligned to the same right hemisphere in all subjects. Accordingly, the subnetworks were designated as follows: (1) the S-S network, representing connections within the surgical hemisphere; and (2) the N-N network, representing connections within the non-surgical hemisphere; (3) the N-S network, representing interhemispheric network. As the connectivity matrices are symmetric, the N-S and S-N networks are identical; therefore, the term N-S network is used throughout this study. All the topological metrics described above were also computed in all subnetworks.

Bootstrap optimism correction and effect size estimation

To assess the potential magnitude of optimism in the in-sample performance estimates, we performed bootstrap optimism correction using 5,000 resamples. The area under the receiver operating characteristic curve (AUC) was used to evaluate the discriminative performance of the MCES. In each bootstrap resample, the logistic regression model used to derive the MCES was refitted, and model discrimination was evaluated both in the bootstrap sample and in the original dataset. The difference between these two AUC estimates was used to quantify optimism, and the mean optimism across all bootstrap iterations was subtracted from the apparent AUC to obtain the optimism-corrected AUC.

For the individual network metrics and AI, bootstrap resampling was used to estimate the mean AUC and 95% confidence interval, and Hedges' g was calculated to quantify the magnitude of group differences. Because these metrics were evaluated directly rather than through a refitted multivariable prediction model, optimism-corrected AUCs were not calculated for them.

Statistical analysis

Gender was compared across the NC, preoperative ICVD, and postoperative ICVD groups using chi-square tests, age was compared using one-way ANOVA. Comparisons involving more than two independent groups were analyzed using Kruskal-Wallis tests followed by Dunn's multiple comparisons test. Independent two-group comparisons were analyzed using two-sample tests, as appropriate. Paired preoperative-postoperative comparisons were analyzed using a paired t-test. In all connectivity analyses, false discovery rate (FDR) correction was applied to p-values using the Benjamini-Hochberg procedure. Only edges surviving FDR correction are displayed. Different thresholds were applied for visualization purposes to improve the clarity of the presented connectivity patterns. Spearman correlation analyses were performed to evaluate the relationship between MCES and clinical scores (NIHSS and mRS), with Bonferroni correction applied for multiple comparisons. All statistical analyses were conducted using SPSS, R, and MATLAB (R2022b).

Results

Participants

The demographic information of all study subjects is shown in Table 1. Among the 31 ICVD subjects, 19 had a left-sided

Table 1 Demographics and characteristics

	NC ($n=17$)	ICVD		*P*-values
		Pre-operation ($n=31$)	Post-operation ($n=21$)	
Age (years)	46.52 ± 9.25	49.13 ± 9.71	48.90 ± 8.84	0.630 [a]
Sex (F/M)	8 / 9	7 / 24	4 / 17	0.112 [b]
Follow-up (days)	\	7.52 ± 2.04		\
NIHSS	\	0 (0–4)	\	\
mRS	\	0 (0–3)	\	\
Blood glucose (mmol/L)	5.98 ± 1.17	5.66 ± 0.62	5.61 ± 0.51	0.287 [a]

[a]The one-way analysis of variance (ANOVA), [b]The Chi-squared test

lesion and underwent left STA-MCA bypass surgery, while 12 had a right-sided lesion and received treatment. There were no significant difference in age, sex, or blood glucose among the groups (all $p>0.05$).

Global network topological alterations in ICVD

Figure 2 shows representative images from two subjects. This patient presented with a marked decrease in metabolic connectivity strength and unilateral hypometabolism before surgery. Twelve days after surgery, metabolism on the operated side remained lower than that on the normal side, but the metabolic connectivity network had changed significantly. Topological indicators also showed an improving trend.

Figure 3a shows the spatial distribution of edges with significantly altered connectivity strength that survived FDR correction in the preoperative ICVD group compared with the NC group. For visualization purposes, only edges with FDR-corrected $p<0.005$ are displayed. The surgical side was adjusted to the right side in all patients in the ICVD preoperative group. Whole-brain metabolic connectivity strength was weaker in the preoperative ICVD group than in the NC group, and most differential connectivity edges involved interhemispheric connections. At the global topological level, the ICVD group showed significant alterations in network properties. MCES and AI differed significantly between the two groups ($p<0.001$). The MCES showed an apparent AUC of 0.922; after bootstrap optimism correction, the AUC was reduced to 0.826. Specifically, B was significantly higher in the preoperative ICVD group than in the NC group ($p<0.001$), whereas C, D, and E_{global} were significantly lower ($p<0.001$). The results suggest that the network integration and information transmission efficiency were decreased in patients with ICVD. Meanwhile, E_{local} was significantly decreased in the ICVD group ($p<0.0001$), whereas L_p was significantly increased ($p<0.0001$), indicating that the overall communication path of the brain network became longer and local information processing was relatively weakened. There were no significant difference in modularity or the hierarchical coefficient between the two groups ($p>0.05$), suggesting that the modular distribution and hierarchical organizational structure remained relatively stable at the global level. Please refer to Supplementary

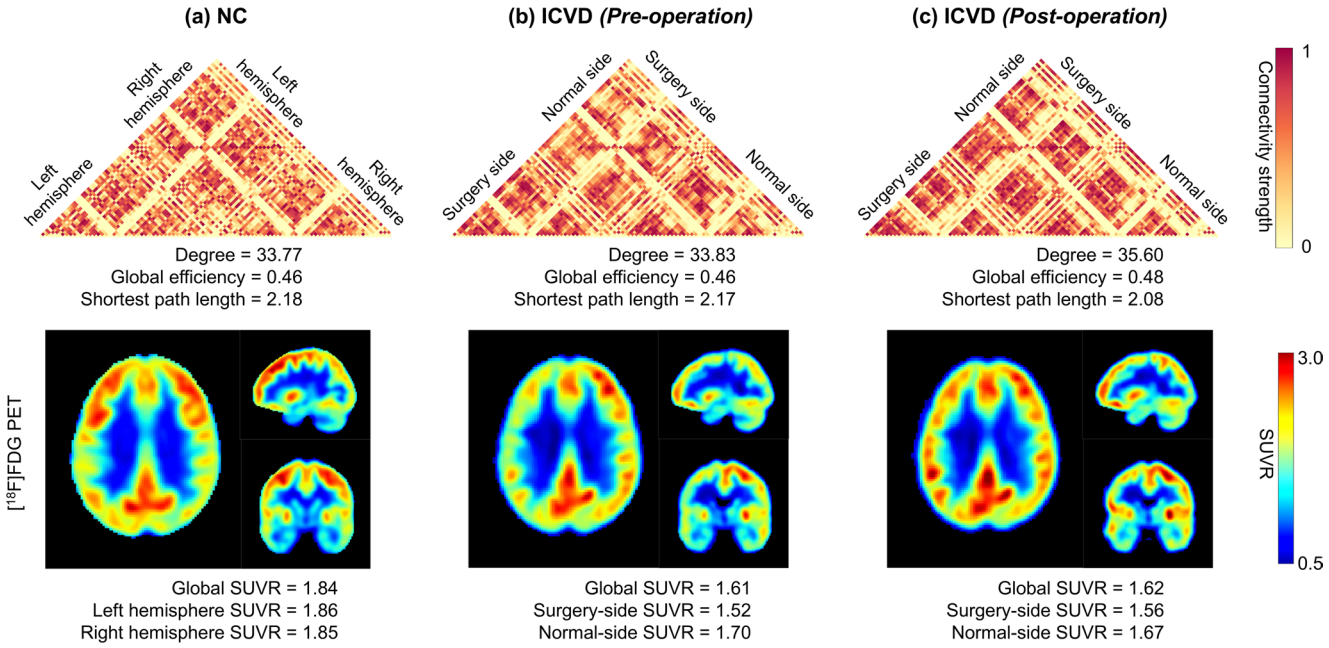


Fig. 2 Metabolic connectivity network and [^{18}F]FDG PET of three typical cases

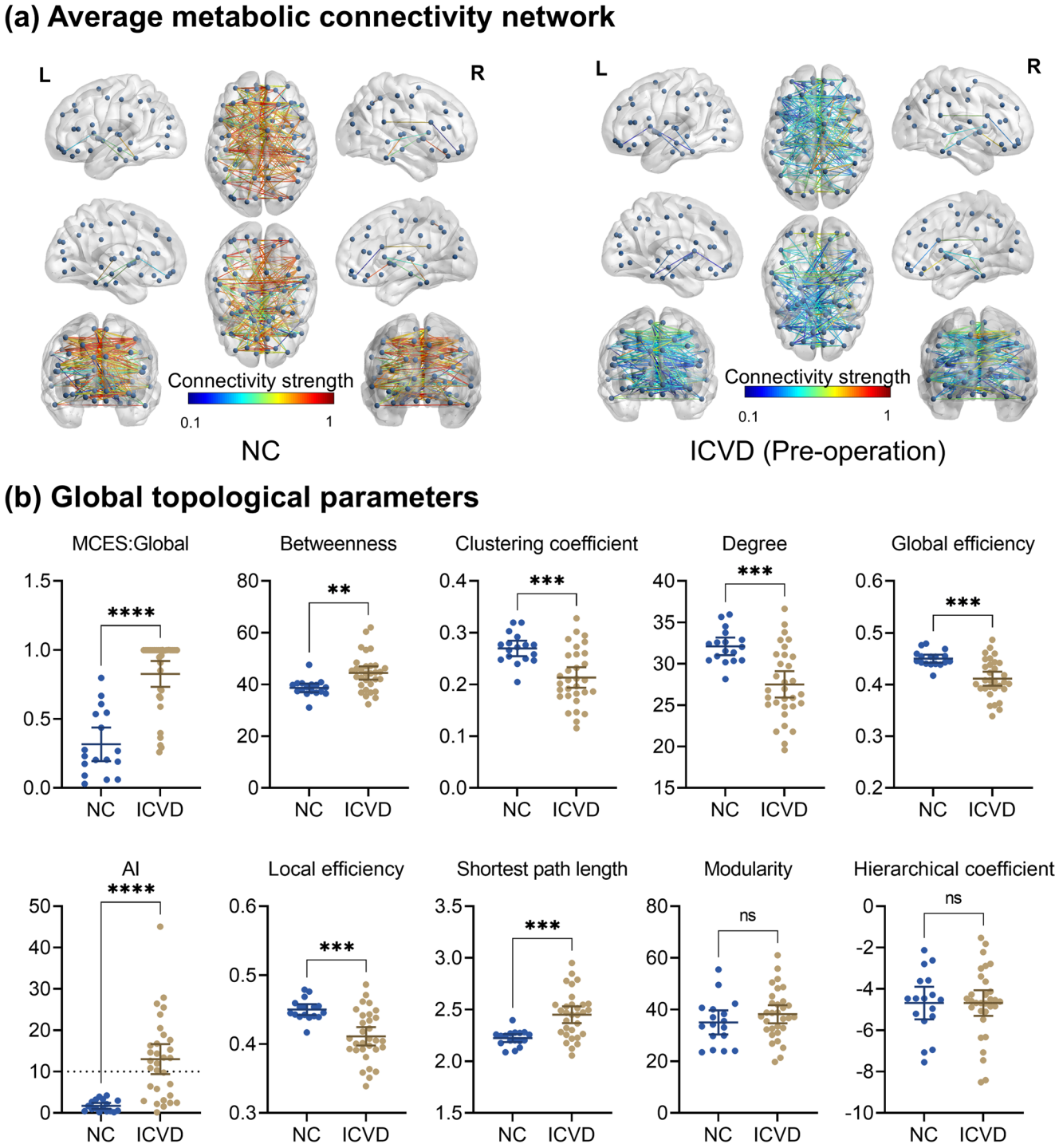


Fig. 3 (**a**) The differential connectivity edges between the NC and ICVD pre-operation group. For visualization purposes, a threshold of FDR-corrected $p < 0.005$ was applied. (**b**) The global parameters in the NC and ICVD pre-operation groups

Table S1 for the bootstrap optimism-corrected discrimination performance of the MCES, and to Supplementary Table S2 for the bootstrap-estimated discrimination performance and Hedges' g effect sizes of individual topological metrics in the global network comparison between NC and preoperative ICVD.

Intrahemispheric topological alterations in ICVD

Figures 4 and 5 show the subnetworks and differences in their parameters. Figure 4a shows that the connection strength of the S-S network was significantly lower than that of the N-N network. All displayed edges survived FDR

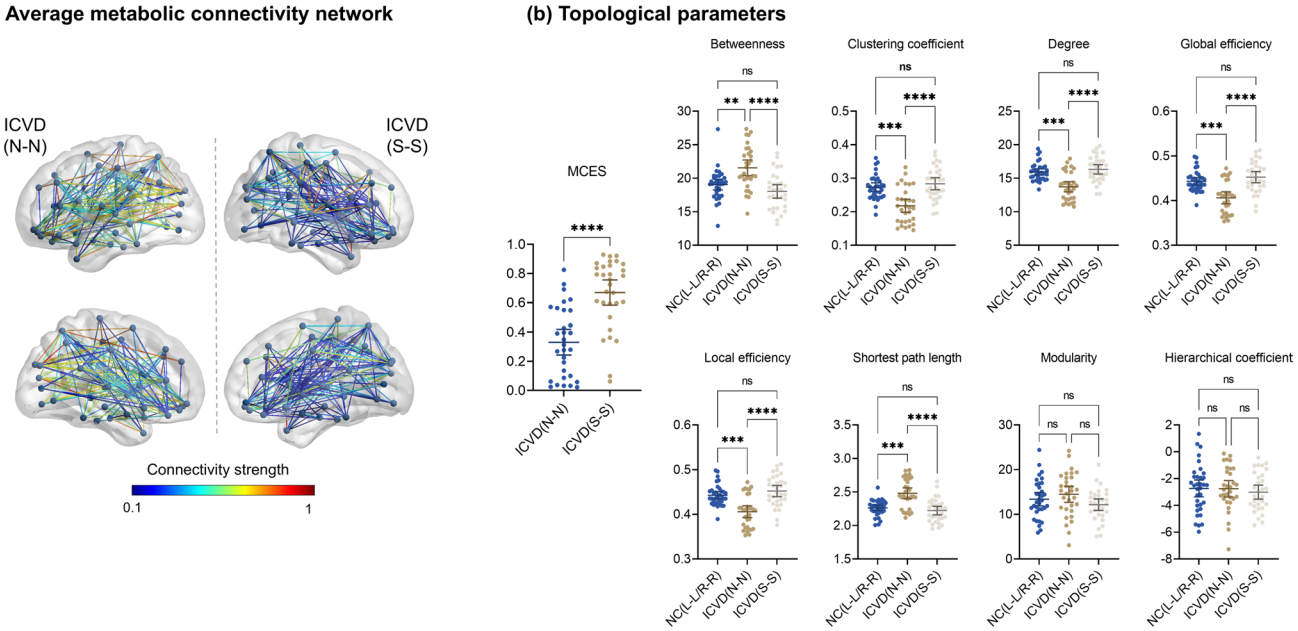


Fig. 4 (**a**) The differential connectivity edges between the N-N network and S-S network in the ICVD pre-operation group. For visualization purposes, a threshold of FDR-corrected $p<0.001$ was applied. (**b**) The subnetwork parameters in the NC and ICVD pre-operation groups

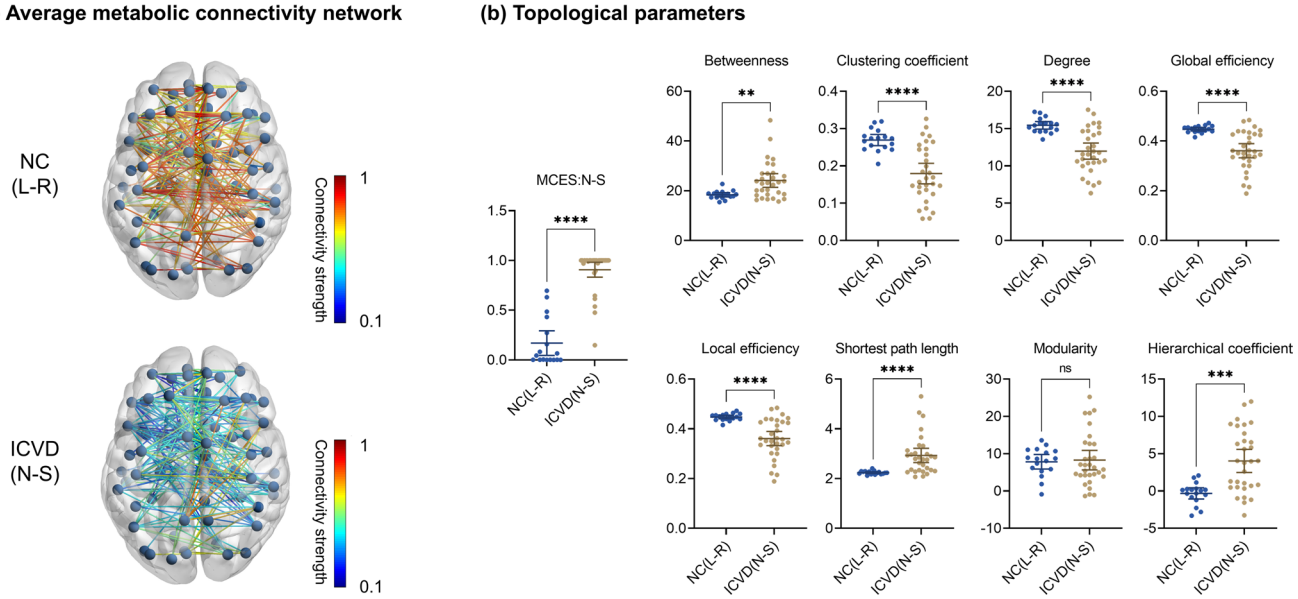


Fig. 5 (**a**) The differential connectivity edges between the N-S network in the ICVD pre-operation group and the L-R network in the NC group. For visualization purposes, a threshold of FDR-corrected $p<0.005$ was applied. (**b**) The subnetwork parameters in the NC and ICVD pre-operation groups

correction. For visualization purposes, a threshold of FDR-corrected $p<0.001$ was applied. Figure 4b further compares differences in topological parameters among the N-N network of the preoperative ICVD group, the S-S network of the preoperative ICVD group, and the L-L/R-R network of the NC group. The results showed that B and L_p in the N-N network of the preoperative ICVD group were significantly higher than those in the NC hemisphere network and S-S network of the preoperative ICVD group ($p<0.01$), whereas C, D, E_{global}, and E_{local} values were significantly lower than those in the NC hemisphere network and S-S network of the preoperative ICVD group ($p<0.001$). Parameters M and H did not differ significantly among the three groups ($p>0.05$). Please refer to Supplementary Table S3 for

the bootstrap-estimated discrimination performance and Hedges' g effect sizes of individual topological metrics in the intrahemispheric network comparison between preoperative ICVD(N-N) and preoperative ICVD(S-S).

Interhemispheric topological alterations in ICVD

Figure 5a shows the distribution of the difference edges between the N-S network in the ICVD group and the L-R network in the NC group; similarly, the N-S network has a lower connection strength. The MCES derived from interhemispheric network reached the highest optimism-corrected AUC of 0.891 shown in the Supplementary Table S1. All displayed edges survived FDR correction. For visualization purposes, only connections with FDR-corrected $p<0.005$ are displayed. B, L_p, and H were significantly higher in the N-S network than the L-R network in the NC, while C, D, E_{global}, and E_{local} values were significantly lower. The parameter M was not significantly different between the two groups. Please refer to Supplementary Table S2 for the bootstrap-estimated discrimination performance and Hedges' g effect sizes of individual topological metrics in the interhemispheric network comparison between NC and preoperative ICVD.

Postoperative longitudinal topological changes in ICVD

The results of the paired t-test of the metabolic connectivity network are shown in Fig. 6a, where the connectivity edges survived FDR correction are shown, with the right side corresponding to the surgical side. A threshold of FDR-corrected $p<0.01$ was applied for visualization. The connectivity strength of the metabolic network in the postoperative group was significantly stronger than that before surgery globally, reflecting the overall improvement after surgery. Further observation revealed that there were more enhanced connections within the normal side than the operated side,

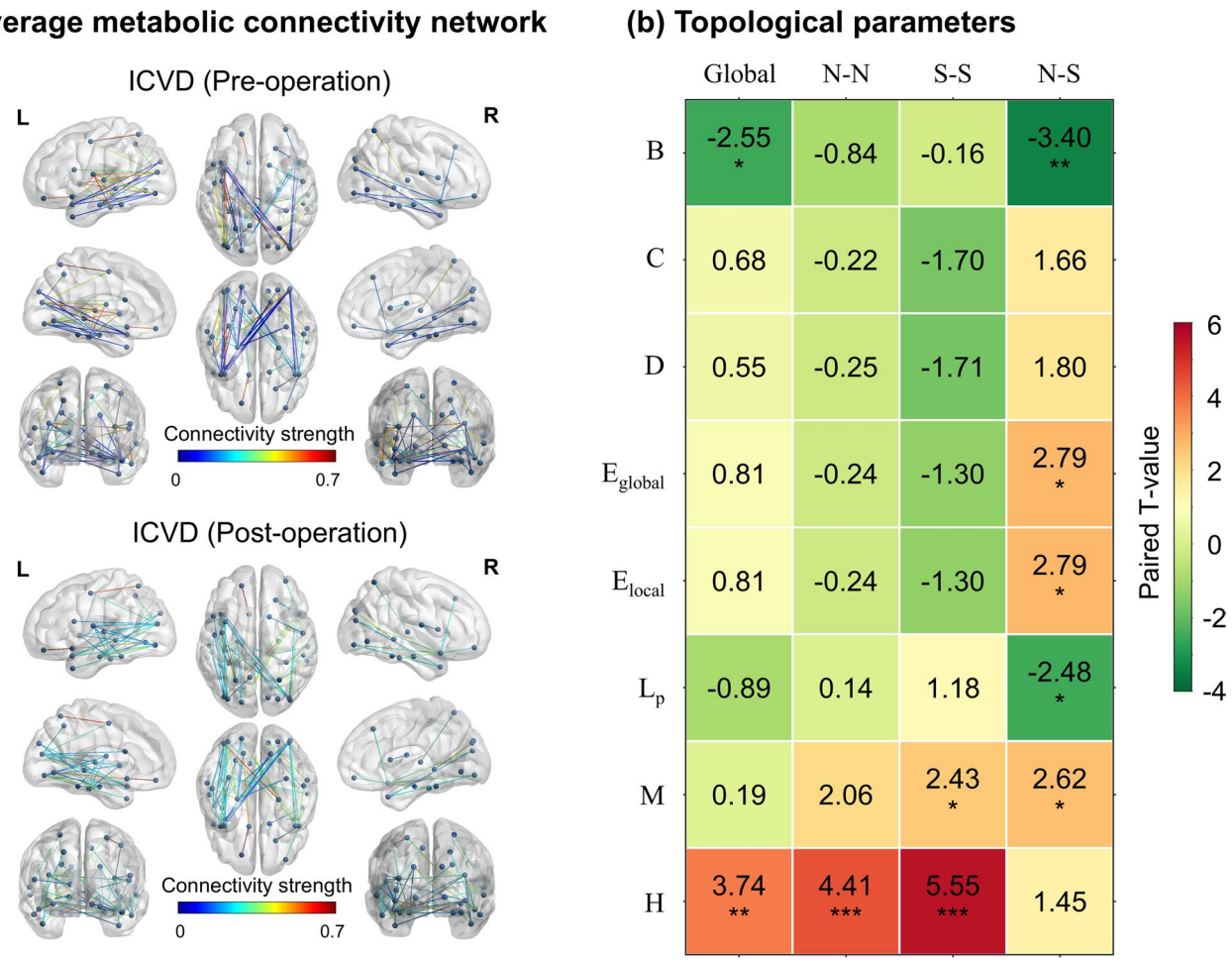


Fig. 6 (**a**) The differential connectivity edges between the ICVD pre-operation group and ICVD post-operation group. For visualization purposes, a threshold of FDR-corrected $p<0.01$ was applied. (**b**) T-map of paired t-test results comparing all types of metabolic networks between the preoperative and postoperative ICVD group

suggesting that the surgery may have triggered a compensatory network reorganization, allowing the normal hemisphere to play a more prominent role in functional integration.

From the perspective of changes in topological parameters, the hierarchical coefficient (H) of the global network, N-N network, and S-S network all increased significantly, even higher than the NC group, as shown in Supplementary Fig. S1a-c. Most indicators of N-S network (including B, C, D, E_{global}, E_{local}, and L_p) also changed significantly towards normal as shown in Fig. 6b and Supplementary Fig. S1d. Please refer to Supplementary Table S4 for the bootstrap-estimated discrimination performance and Hedges' g effect sizes of individual topological metrics in the comparison between preoperative ICVD and postoperative ICVD.

In addition, we selected subjects at different postoperative time points to observe dynamic changes in the metabolic network, as shown in Supplementary Fig. S2. The average connectivity network of the NC group was used as a reference. The results revealed that overall connection strength changed continuously over time after surgery. On postoperative day 3, the patients showed the greatest difference from the NC group, particularly in several connections associated with the left superior temporal gyrus. As recovery progressed, these connections gradually showed a trend toward normalization; however, even on postoperative day 12, the overall connectivity strength distribution had not fully returned to the normal level. The full names of the brain regions shown in the figure are provided in Supplementary Table S5.

Correlation analysis

Supplementary Fig. S3 illustrates the correlations between MCES and clinical scales, with p-values corrected using the Bonferroni method. Significant correlations were observed between MCES and NIHSS in the global, N-N, and N-S networks of the preoperative ICVD group ($|r|=0.582\sim0.650$, $p<0.05$), whereas no significant correlation was found in the S-S network. In contrast, MCES showed no significant correlation with mRS in any network ($p>0.05$).

Discussion

This study aims to establish individualized metabolic networks using [^{18}F]FDG PET to investigate metabolic connectivity alterations associated with surgical revascularization in patients with ICVD. Against the backdrop of PET/MR serving as a noninvasive imaging tool for probing hemodynamic and metabolic alterations pre- and post-bypass surgery, we compared the topological characteristics among the preoperative ICVD group, postoperative ICVD group, and normal control group, aiming to elucidate the alteration patterns of metabolic connectivity associated with unilateral ICA or MCA occlusive or stenotic disease-particularly for MR-negative regions identified on structural images. Our findings provide exploratory evidence that individualized metabolic connectivity may serve as a complementary imaging approach for evaluating early postoperative metabolic network changes following cerebral revascularization.

Our results demonstrated characteristic patterns of cerebral network injury in patients with ICVD before surgery. Compared with the NC group, the preoperative ICVD group exhibited significantly reduced whole-brain metabolic connectivity strength, with most differential connectivity edges localized to interhemispheric connections. At the global topological level, marked alterations were observed: MCES and AI differed significantly between the groups, with the preoperative ICVD group showing a significantly higher B value and lower C, D, and E_{global} values. The apparent MCES performance was optimistic, but the corrected estimates still suggested exploratory group-level discrimination, particularly for interhemispheric network. These changes reflect impaired network integration and reduced efficiency of information transmission, consistent with previous reports of hemodynamic and metabolic disturbances induced by chronic cerebral hypoperfusion [23, 24]. Furthermore, E_{local} was significantly decreased and L_p was significantly prolonged in the ICVD group, indicating longer brain network communication paths and weakened local information processing capacity, key manifestations of ischemic injury-induced disruption of the structural integrity and functional coordination of neural circuits. Barbara et al. demonstrated that metabolic networks constructed using [^{18}F]FDG PET can serve as robust systemic biomarkers of metabolic homeostasis that enable the quantification of homeostatic load, reveal the transition from health to disease, and provide a novel framework for clinical health assessment [25]. Philipp et al. found that lesion-induced disruption of large-scale brain metabolic networks occurs in patients with severe stroke and that this mechanism may play a key role in stroke recovery [26]. Notably, no significant differences were detected in modularity and hierarchical coefficient between the preoperative ICVD and NC groups, suggesting that the core modular distribution and hierarchical organization of the cerebral network may remain relatively stable in early ICVD. This finding may be consistent with the neural remodeling theory, suggesting that post-injury plasticity is associated with the preservation of original neural structures. The observed preservation of network integrity may therefore represent an early feature of postoperative metabolic network reorganization. Similar preservation of the core network framework has been

reported in chronic stroke studies, where it predicts favorable functional recovery potential [27, 28].

Surgical intervention represents a cornerstone in the clinical management of stroke, although the mechanisms underlying postoperative brain reorganization remain incompletely understood. Liu et al. pioneered the concept of the "molecular window" for ischemic stroke intervention, a paradigm that fundamentally transcends the spatiotemporal constraints inherent in the conventional time-window framework. Rather than confining therapeutic strategies to the acute reperfusion phase, this concept extends the therapeutic horizon to targeted modulation of the persistent molecular pathological cascades that continue to propagate in the post-ischemic brain [29]. Our findings provide exploratory neuroimaging-based evidence of early postoperative metabolic network changes following surgical revascularization in ICVD. Although these observations should not be interpreted as evidence of long-term functional recovery or therapeutic efficacy, they suggest that individualized metabolic network analysis may offer a complementary approach for characterizing early metabolic reorganization after surgery. After STA-MCA bypass surgery, the metabolic connectivity network showed postoperative reorganization toward a more normalized pattern. Globally, metabolic connectivity strength was significantly stronger in the postoperative group than in the preoperative group, suggesting a trend toward partial normalization of the metabolic network after revascularization. Consistent with previous hemodynamic studies, the interhemispheric (N-S) network showed significant normalization of topological parameters, including B, C, D, E_{global}, E_{local}, and L_p. These findings may be compatible with neural remodeling theory, which proposes that, following cerebral ischemia, neural tissue preferentially repairs network connectivity through remodeling strategies such as synaptic regeneration, axonal sprouting, and circuit reorganization, rather than simply restoring local metabolism. In our cohort, early postoperative alterations in metabolic network organization were observed despite incomplete recovery of local metabolic levels in the operated hemisphere. This observation is consistent with serial PET studies showing that glucose metabolism recovery is delayed relative to perfusion improvement [30]. Importantly, postoperative enhancement of intrahemispheric connections was more pronounced in the non-surgical hemisphere than in the surgical hemisphere. This phenomenon may reflect differential network reorganization between the two hemispheres during the early postoperative period, which may be associated with functional redistribution following lesions in the affected hemisphere. This finding may be consistent with the theory of "contralateral compensatory mechanism" in the neural remodeling in ICVD, analogous to hemodynamic observations in carotid endarterectomy patients, where CBF improvements were noted in both hemispheres. Previous clinical neuroimaging studies on patients more heavily affected by stroke primarily reported a reduction of interhemispheric connections, observed for both activation tasks and at rest [31, 32]. Most interesting, studies on severely affected stroke patients with subcortical lesions described both clustering coefficient and characteristic path length to decrease during recovery, suggesting a more random network topology [33, 34]. The post-operative enhancement of metabolic connectivity networks, improvement of topological parameters, and alterations in network characteristics observed in the non-surgical hemisphere provide exploratory imaging evidence of early metabolic network changes following revascularization. Compared with traditional metabolic level assessment, changes in topological parameters may provide additional information to reflect the stimulatory effect of surgery on metabolic network organization during the early postoperative period. Because neurological scores obtained in the immediate postoperative period may be influenced by transient surgery-related factors and early recovery status, the relationship between metabolic network reorganization and clinical outcomes should be further validated using long-term follow-up assessments.

Several limitations of this study should be acknowledged. First, this was a single-center study with a relatively small sample size, which may reduce the generalizability of the conclusions. Second, follow-up data were lacking, including short-term follow-up data for ten participants and long-term follow-up data for all participants, which may introduce potential selection bias and affect the generalizability of the longitudinal findings. In particular, the absence of long-term follow-up limited our ability to determine whether the favorable metabolic network reorganization could be sustained over time and how these alterations correlate with long-term neurological functional recovery. Third, the evidence for neural remodeling mechanisms, including synaptic regeneration and axonal sprouting, was indirectly inferred from metabolic network topology, without direct validation by histopathological, molecular, or electrophysiological methods, and the precise biological mechanisms underlying network repair remain to be further explored.

Conclusions

This study analyzed cerebral metabolic connectivity in ICVD patients by [^{18}F]FDG PET. Preoperatively, patients exhibited reduced whole-brain metabolic connectivity and disrupted network topology. Following STA-MCA bypass, the metabolic network demonstrated early postoperative reorganization, including enhanced global connectivity,

partial normalization of interhemispheric topology, and increased compensatory intrahemispheric connectivity in the non-surgical hemisphere. These findings suggest that graph-theoretical measures of metabolic connectivity may provide insight into early postoperative metabolic network reorganization. Further studies with larger cohorts, longer follow-up, and postoperative functional outcome assessments are warranted to determine their clinical significance.

Supplementary Information The online version contains supplementary material available at https://doi.org/10.1007/s00259-026-08083-y.

Author contributions All authors have made substantial contributions in all 3 of the following categories: (1) Contributing to conception and design, or acquiring data, or analyzing and interpreting data; (2) Drafting the manuscript, or critically contributing to or revising the manuscript, or enhancing its intellectual content; and (3) Approving the final content of the manuscript. Detailed contributions from all authors are provided below: B.C., Q.Z., and Y.S.: Formal analysis, Methodology, Visualization, Writing - original draft. J.M.: Data curation, Validation, Writing - review & editing. X.W., Y.X., and J.J.J.: Data curation, Visualization, Writing - review & editing. L.W., M.B., A.R., and K.S.: Conceptualization, Supervision, Writing - review & editing. M.W., J.H.J., and J.L.: Conceptualization, Project administration, Supervision, Writing - review & editing.

Funding This study was supported by Project supported by Beijing Natural Science Foundation (Grant No.7254540), Noncommunicable Chronic Diseases-National Science and Technology Major Project (Grant No. 2024ZD0539800), Beijing Physician Scientist Training Project (BJPSTP-2025-30), the National Natural Science Foundation of China (62303295, 62376150), Shanghai Pujiang Talents Program (24PJD039). Matthias Brendel was funded by the Deutsche Forschungsgemeinschaft (DFG) under Germany's Excellence Strategy within the framework of the Munich Cluster for Systems Neurology (EXC 2145 SyNergy, ID 390857198).

Data availability The data generated and analyzed during the current study are available from the corresponding author on reasonable request.

Declarations

Ethics approval All procedures performed in studies involving human participants were in accordance with the ethical standards of the institutional and/or national research committee and with the 1964 Helsinki Declaration and its later amendments or comparable ethical standards. The study was approved by the ethics committee and institutional review board of Xuanwu Hospital (Approval number: [2025]286-002).

Consent to participate Written informed consent was obtained from all participants before the examinations.

Competing interests Axel Rominger and Kuangyu Shi are editors of this journal. Matthias Brendel is a member of the Neuroimaging Committee of the EANM. Matthias Brendel has received speaker honoraria from Roche, GE Healthcare, Iba, Miltenyi and Life Molecular Imaging; has advised Life Molecular Imaging, MIAC, Cenos and GE healthcare; and is currently on the advisory or imaging review boards of AC Immune and ZRO Imaging.

References

1. Palaniappan LP, Allen NB, Almarzooq ZI, Anderson CAM, Arora P, Avery CL, et al. 2026 Heart disease and stroke statistics: a report of us and global data from the American Heart Association. Circulation. 2026;153:e275–906. https://doi.org/10.1161/CIR.0000000000001412
2. Feigin VL, Stark BA, Johnson CO, Roth GA, Bisignano C, Abady GG, et al. Global, regional, and national burden of stroke and its risk factors, 1990–2019: a systematic analysis for the Global Burden of Disease Study 2019. Lancet Neurol. 2021;20:795–820. https://doi.org/10.1016/S1474-4422(21)00252-0.
3. Teng P, Wang Y-Y, Ding C-Y, Huang J-J, Nie R, Liu N, et al. Dynamics and heterogeneity of the neurovascular unit in ischemic stroke. Trends Pharmacol Sci. 2026;47:423–38. https://doi.org/10.1016/j.tips.2026.01.005.
4. Bennett HC, Zhang Q, Wu Y, Manjila SB, Chon U, Shin D, et al. Aging drives cerebrovascular network remodeling and functional changes in the mouse brain. Nat Commun. 2024;15:6398. https://doi.org/10.1038/s41467-024-50559-8.
5. Blaschke SJ, Hensel L, Minassian A, Vlachakis S, Tscherpel C, Vay SU, et al. Translating Functional Connectivity After Stroke: Functional Magnetic Resonance Imaging Detects Comparable Network Changes in Mice and Humans. Stroke. 2021;52:2948–60. https://doi.org/10.1161/STROKEAHA.120.032511.
6. Vesey AT, Jenkins WSA, Irkle A, Moss A, Sng G, Forsythe RO, et al. 18 F-Fluoride and18 F-Fluorodeoxyglucose positron emission tomography after transient ischemic attack or minor ischemic stroke: case–control study. Circ: Cardiovasc Imaging. 2017;10:e004976. . https://doi.org/10.1161/CIRCIMAGING.116.004976
7. Liang Y, Cui B, Ye L, Yang B, Shan Y, Yang H, et al. Comparison of the Correlation Between Cerebral [18F]FDG Metabolism as Assessed by Two Asymmetry Indices and Clinical Neurological Score in Patients with Ischemic Cerebrovascular Disease. Mol Imaging Biol. 2025;27:454–64. https://doi.org/10.1007/s11307-025-02002-7.
8. Lee R, Choi H, Park K-Y, Kim J-M, Seok JW. Prediction of post-stroke cognitive impairment using brain FDG PET: deep learning-based approach. Eur J Nucl Med Mol Imaging. 2022;49:1254–62. https://doi.org/10.1007/s00259-021-05556-0.
9. Huang C, Mattis P, Tang C, Perrine K, Carbon M, Eidelberg D. Metabolic brain networks associated with cognitive function in Parkinson's disease. NeuroImage. 2007;34:714–23. https://doi.org/10.1016/j.neuroimage.2006.09.003.
10. Wang M, Jiang J, Yan Z, Alberts I, Ge J, Zhang H, et al. Individual brain metabolic connectome indicator based on Kullback-Leibler Divergence Similarity Estimation predicts progression from mild cognitive impairment to Alzheimer's dementia. Eur J Nucl Med Mol Imaging. 2020;47:2753–64. https://doi.org/10.1007/s00259-020-04814-x.
11. Yakushev I, Drzezga A, Habeck C. Metabolic connectivity: methods and applications. Curr Opin Neurol. 2017;30:677–85. https://doi.org/10.1097/WCO.0000000000000494.
12. Zhang Q, Li F, Wei M, Wang M, Wang L, Han Y, et al. Prediction of Cognitive Progression Due to Alzheimer's Disease in Normal Participants Based on Individual Default Mode Network Metabolic Connectivity Strength. Biol Psychiatry: Cogn Neurosci Neuroimaging. 2024;9:660–7. https://doi.org/10.1016/j.bpsc.2024.04.004.
13. Rust R, Nih LR, Liberale L, Yin H, El Amki M, Ong LK, et al. Brain repair mechanisms after cell therapy for stroke. Brain. 2024;147:3286–305. https://doi.org/10.1093/brain/awae204.
14. Grefkes C, Fink GR. Reorganization of cerebral networks after stroke: new insights from neuroimaging with connectivity

approaches. Brain. 2011;134:1264–76. https://doi.org/10.1093/brain/awr033.
15. Bullmore E, Sporns O. Complex brain networks: graph theoretical analysis of structural and functional systems. Nat Rev Neurosci Springer Sci Bus Media LLC. 2009;10:186–98. https://doi.org/10.1038/nrn2575.
16. Tuan PM, Horowitz T, Adel M, Wojak J, Trung NL, Guedj E. Comparative evaluation of graph construction methods for individual brain metabolic network from FDG-PET images: an ADNI study in healthy subjects. Eur J Nucl Med Mol Imaging. 2025;53:1139–54. https://doi.org/10.1007/s00259-025-07462-1.
17. Hu D, Dou X, Wang J, Jin C, Liu K, Zhou R, et al. A novel approach of [18F]FDG PET-based individual metabolic radiomics network to predict cognitive impairment in multiple system atrophy. NeuroImage. 2025;319:121433. https://doi.org/10.1016/j.neuroimage.2025.121433.
18. Stockbauer A, Beyer L, Huber M, Kreuzer A, Palleis C, Katzdobler S, et al. Metabolic network alterations as a supportive biomarker in dementia with Lewy bodies with preserved dopamine transmission. Eur J Nucl Med Mol Imaging. 2024;51:1023–34. https://doi.org/10.1007/s00259-023-06493-w.
19. Vallini G, Silvestri E, Volpi T, Lee JJ, Vlassenko AG, Goyal MS, et al. Individual-level metabolic connectivity from dynamic [18F] FDG PET reveals glioma-induced impairments in brain architecture and offers novel insights beyond the SUVR clinical standard. Eur J Nucl Med Mol Imaging. 2025;52:836–50. https://doi.org/10.1007/s00259-024-06956-8.
20. Wang M, Cui B, Shan Y, Yang H, Yan Z, Sundar LKS, et al. Non-Invasive Glucose Metabolism Quantification Method Based on Unilateral ICA Image Derived Input Function by Hybrid PET/MR in Ischemic Cerebrovascular Disease. IEEE J Biomed Health Inf. 2022;26:5122–9. https://doi.org/10.1109/JBHI.2022.3193190.
21. Liang Y, Cui B, Ye L, Yang B, Shan Y, Yang H, et al. Comparison of the Correlation Between Cerebral [18F]FDG Metabolism as Assessed by Two Asymmetry Indices and Clinical Neurological Score in Patients with Ischemic Cerebrovascular Disease. Mol Imaging Biol. 2025;27:454–64. https://doi.org/10.1007/s11307-025-02002-7.
22. Tzourio-Mazoyer N, Landeau B, Papathanassiou D, Crivello F, Etard O, Delcroix N, et al. Automated Anatomical Labeling of Activations in SPM Using a Macroscopic Anatomical Parcellation of the MNI MRI Single-Subject Brain. NeuroImage. 2002;15:273–89. https://doi.org/10.1006/nimg.2001.0978.
23. Park J-H, Hong J-H, Lee S-W, Ji HD, Jung J-A, Yoon K-W, et al. The effect of chronic cerebral hypoperfusion on the pathology of Alzheimer's disease: A positron emission tomography study in rats. Sci Rep. 2019;9:14102. https://doi.org/10.1038/s41598-019-50681-4.
24. Lee J-I, Lim JS, Hong J-H, Kim S, Lee S-W, Ji HD et al. Selective neurodegeneration of the hippocampus caused by chronic cerebral hypoperfusion: F-18 FDG PET study in rats. Mongin AA, editor. PLoS ONE. 2022;17:e0262224. https://doi.org/10.1371/journal.pone.0262224
25. Geist BK, Guthrie J, Kertesz H, Kiefer FW, Kulterer OC, Nakuz T, et al. The metabolic organ connectome: A novel approach to measure allostatic load during health-to-disease transition. Med. 2025;6:100881. https://doi.org/10.1016/j.medj.2025.100881.
26. Koch PJ, Frey BM, Backhaus W, Petersen N, Girard G, Wróbel PP, et al. Neurotransmitter-informed connectivity maps and their application for outcome inference after stroke. Brain. 2025;148:3935–45. https://doi.org/10.1093/brain/awaf185.
27. Di Pino G, Pellegrino G, Assenza G, Capone F, Ferreri F, Formica D, et al. Modulation of brain plasticity in stroke: a novel model for neurorehabilitation. Nat Rev Neurol Nat Publishing Group. 2014;10:597–608. https://doi.org/10.1038/nrneurol.2014.162.
28. Allegra Mascaro AL, Conti E, Lai S, Di Giovanna AP, Spalletti C, Alia C, et al. Combined Rehabilitation Promotes the Recovery of Structural and Functional Features of Healthy Neuronal Networks after Stroke. Cell Rep. 2019;28:3474–e34856. https://doi.org/10.1016/j.celrep.2019.08.062.
29. Liu Q, Wu C, Fisher M, Wu D, Ji X. Molecular windows for ischemic stroke treatment. Sci Bull. 2025;70:2714–6. https://doi.org/10.1016/j.scib.2025.06.032.
30. Wang Q, Bie F, Lu T, Sun X, Sun Q, Wang G, et al. The effect of cerebral blood perfusion on the correlation between cerebral stroke onset time and synthetic T2 mapping: a pilot study. Quant Imaging Med Surg. 2023;13:3477–88. https://doi.org/10.21037/qims-22-991.
31. Adhikari MH, Griffis J, Siegel JS, Thiebaut De Schotten M, Deco G, Instabato A, et al. Effective connectivity extracts clinically relevant prognostic information from resting state activity in stroke. Brain Commun. 2021;3:fcab233. https://doi.org/10.1093/braincomms/fcab233.
32. Frontzkowski L, Fehring F, Frey BM, Wróbel PP, Reibelt A, Higgen F, et al. Frontoparietal Structural Network Disconnections Correlate With Outcome After a Severe Stroke. Hum Brain Mapp. 2024;45:e70060. https://doi.org/10.1002/hbm.70060.
33. Yourganov G, Stark BC, Fridriksson J, Bonilha L, Rorden C. Effect of Stroke on Contralateral Functional Connectivity. Brain Connect. Mary Ann Liebert Inc publishers. 2021;11:543–52. https://doi.org/10.1089/brain.2020.0901.
34. Braaß H, Gutgesell L, Backhaus W, Higgen FL, Quandt F, Choe C, et al. Early functional connectivity alterations in contralesional motor networks influence outcome after severe stroke: a preliminary analysis. Sci Rep. 2023;13:11010. https://doi.org/10.1038/s41598-023-38066-0.

Publisher's Note Springer Nature remains neutral with regard to jurisdictional claims in published maps and institutional affiliations.

Springer Nature or its licensor (e.g. a society or other partner) holds exclusive rights to this article under a publishing agreement with the author(s) or other rightsholder(s); author self-archiving of the accepted manuscript version of this article is solely governed by the terms of such publishing agreement and applicable law.

Authors and Affiliations

Bixiao Cui[1,2,3,4] · Qi Zhang[5,6] · Yi Shan[1,3,4] · Xinyu Wei[6] · Yaqi Xu[6] · Jie Ma[1,2,3] · Juanjuan Jiang[7] · Luyao Wang[6] · Matthias Brendel[8,9,10] · Axel Rominger[11] · Kuangyu Shi[11,12] · Min Wang[6] · Jiehui Jiang[6] · Jie Lu[1,3,4]

✉ Min Wang
wmwin@shu.edu.cn

✉ Jiehui Jiang
jiangjiehui@shu.edu.cn

✉ Jie Lu
imaginglu@hotmail.com

1 Department of Radiology and Nuclear Medicine, Xuanwu Hospital, Capital Medical University, Beijing, China

2 Beijing Engineering Research Center of Radiographic Techniques and Equipment, Institute of High Energy Physics, Chinese Academy of Sciences, Beijing, China

3 Beijing Key Laboratory of Innovation and Translation of Central Nervous System Radiopharmaceuticals, Beijing, China

4 Beijing Key Laboratory of Magnetic Resonance Imaging and Brain Informatics, Beijing, China

5 School of Communication & Information Engineering, Shanghai University, Shanghai, China

6 Institute of Biomedical Engineering, School of Life Sciences, Shanghai University, Shanghai, China

7 School of Medical Imaging, Shanghai University of Medicine and Health Science, Shanghai, China

8 Department of Nuclear Medicine, LMU University Hospital, LMU Munich, Munich, Germany

9 German Center for Neurodegenerative Diseases (DZNE), Munich, Germany

10 Munich Cluster for Systems Neurology (SyNergy), Munich, Germany

11 Department of Nuclear Medicine, Inselspital, University Hospital Bern, Bern, Switzerland

12 Department of Informatics, Technische Universität München, Munich, Germany